Electron-impact excitation of the Ba^+ ion*

D. H. Crandall, Paul O. Taylor, and Gordon H. Dunn†

Joint Institute for Laboratory Astrophysics, University of Colorado and National Bureau of Standards, Boulder, Colorado 80302

(Received 14 March 1974)

Crossed beams of Ba^+ and electrons were used to measure the absolute emission cross sections for the Ba^+ lines, 455.4, 493.4, 490.0, and 413.1+416.6 nm. Polarization fractions of the light were also measured. The data were analyzed to extract level excitation cross sections. The excitation cross section for the $6\,^2P_{3/2}$ level has a value 34.7×10^{-16} cm^2 at the 2.72-eV threshold, shows marked structure in the 3–10-eV interval, and decreases to 1.71×10^{-16} cm^2 at 747 eV. The polarization fraction for the 455.4-nm light exhibits pronounced oscillatory structure in the interval 3–7 eV. Excitation cross section for the $6\,^2P_{1/2}$, $7\,^2S_{1/2}$, and $6\,^2D_{3/2+5/2}$ levels have values at threshold of 20.0×10^{-16}, 5.4×10^{-16}, and 4.3×10^{-16} cm^2, respectively. Total uncertainties at a "high-confidence level" are about $\pm10\%$ for the $6\,^2P_{1/2}$ and $6\,^2P_{3/2}$ cross sections. Uncertainties range around $\pm30\%$ for the $7\,^2S_{1/2}$ cross section and $\pm20\%$ for the $6\,^2D_{3/2+5/2}$. Measurements for the $6\,^2P$ cross sections agree at high energies with the Coulomb distorted-wave calculation of Sheorey and Burgess. Measurements for the $6\,^2P_{3/2}$ level are in quite good agreement with the measurements of Bacon and Hooper and of Pace and Hooper for energies 6 to 100 eV. However, the Pace and Hooper points at 3 and 4 eV are nearly twice the present values. Signals due to excitation of metastable $5\,^2D$ ions in the ion beam were observed, and estimates could be made of the cross section for excitation from this state to the final states above. Cross secitons at threshold were estimated to be 13.4×10^{-16} cm$^2\pm34\%$, 9.8×10^{-16} cm$^2\pm28\%$, 7.4×10^{-16} cm$^2\pm100\%$, 6.9×10^{-16} cm$^2\pm27\%$ for excitation from the $5\,^2D$ levels to the $6\,^2P_{3/2}$, $6\,^2P_{1/2}$, $7\,^2S_{1/2}$, and $6\,^2D_{5/2+3/2}$ levels, respectively. The rate coefficients for excitaiton of $6\,^2P_{3/2}$ calcualted from the data are in reasonable agreement with the measurements of Hinnov *et al.*

I. INTRODUCTION

Cross sections for electron-impact excitation of ions are theoretically[1] finite—and often a maximum—at threshold; and radiation from ions is frequently used[2] for study of plasma properties. Yet, it is only recently that the crossed-charged-beams technique[3–5] has opened the way for direct measurements of these important cross sections. Published absolute emission cross-section measurements are limited to those[6–11] on N_2^+, Ba^+, Ca^+, Ar^+, and Kr^+. There are also relative measurements[12,13] on He^+.

In this paper we report measurements of absolute cross sections for four Ba^+ emissions. Figure 1 shows an energy-level diagram of Ba^+ indicating the four emissions, 455.4, 493.4, 490.0, and 413.1 +416.6 nm, for which the cross sections were measured as a function of electron impact energy from below threshold to 750 eV. Polarization fractions of the radiation were also measured and are reported here.

After considerable analysis of the emission data, we extract excitation cross sections. Reasonably accurate values for the $6\,^2S_{1/2}\rightarrow6\,^2P_{1/2}$ and $6\,^2S_{1/2}\rightarrow6\,^2P_{3/2}$ excitations as a function of electron energy are obtained which have had cascade and metastable contributions subtracted. Less accurate values of the $6\,^2S_{1/2}\rightarrow7\,^2S_{1/2}$ and $6\,^2S_{1/2}\rightarrow6\,^2D_{3/2+5/2}$ (no cascade correction) are obtained. Further, because of the presence of metastables in the ion beam, we are able to make estimates of the excitation cross sections at the threshold energies for the $5\,^2D\rightarrow6\,^2P_{1/2}$, $5\,^2D\rightarrow6\,^2P_{3/2}$, $5\,^2D\rightarrow7\,^2S$, and $5\,^2D\rightarrow6\,^2D$ transitions.

Results for the $6\,^2P_{3/2}$ level are related and compared to the previous measurements of Bacon and Hooper[7] and Pace and Hooper.[8] The present work adds to the previous measurements: higher precision, greater accuracy, extended energy range, and a finer energy mesh revealing structure in the cross sections. Excitation rate coefficients are calculated from the measured cross sections and compared with the measurements of Hinnov *et al.*[14]

There has been some theoretical interest in electron-impact excitation of Ba^+. The Coulomb distorted-wave calculations of Burgess and Sheorey[15] and the Coulomb-Born work of Petrini[16] are compared with the present results.

II. EXPERIMENTAL TECHNIQUE AND APPARATUS

Basically, the technique and apparatus are the same as used in studies[9] of Ca^+ excitation. The extension of excitation studies from Ca^+ to Ba^+ was not difficult experimentally. The apparatus required no modification; the same ion source, electron gun, and optical detection system were employed without change, and the optical calibration was performed simultaneously for Ca^+ and Ba^+. Therefore, the Ca^+ work[9,17] and a report

on the magnetically confined electron source[18] are significant references for the present work.

Apparatus arrangement and measurement technique are schematically illustrated in Fig. 2. Generally, the procedure is to bombard a beam of Ba^+ ions travelling in the x direction with a beam of variable-energy electrons going in the y direction and count the resultant photons of a given wavelength emitted in a cone along the z axis.

The cross section σ is calculated from experimental quantities using the expression

$$\sigma = \frac{1}{Y_\Omega}\frac{\mathcal{R}}{I_i I_e}\frac{e^2 v_i v_e}{(v_i^2+v_e^2)^{1/2}}\frac{\mathcal{F}}{D(z_0,\lambda)}, \tag{1}$$

where $\mathcal{R}$ is the photon signal count rate, e the electronic charge, I_i and I_e are the ion- and electron-beam currents, respectively, and v_i and v_e are the respective particle velocities. The effect of anisotropy of the emitted radiation on the observed signal is accounted for in terms of the polarization of the radiation, P, by a factor Y_Ω given by

$$Y_\Omega = (1 - P\langle\cos^2\theta\rangle_\Omega)/(1 - \tfrac{1}{3}P), \tag{2}$$

where $\langle\cos^2\theta\rangle_\Omega$ is the value of $\cos^2\theta$ averaged over the detection solid angle. The quantity $D(z_0,\lambda)$ is the absolute average probability that a photon of wavelength λ emitted from a plane at $z=z_0$ within the collision volume will be detected. The variations of sensitivity with position from which the ion radiates are included in the form factor $\mathcal{F}$, given by

$$\mathcal{F} = \frac{\int R(z)\,dz \int G(z)\,dz}{\int R(z)G(z)\eta(z,\lambda)\,dz}, \tag{3}$$

where $R(z)$ and $G(z)$ are spatial distributions of ion and electron beams, and $\eta(z,\lambda)$ is the spatial variation of the sensitivity of the photon detection system.

Techniques for measurement of the quantities in Eqs. (1) and (3) have been discussed previously,[9,17,18] and further discussion here will be limited to features peculiar to the Ba^+ work.

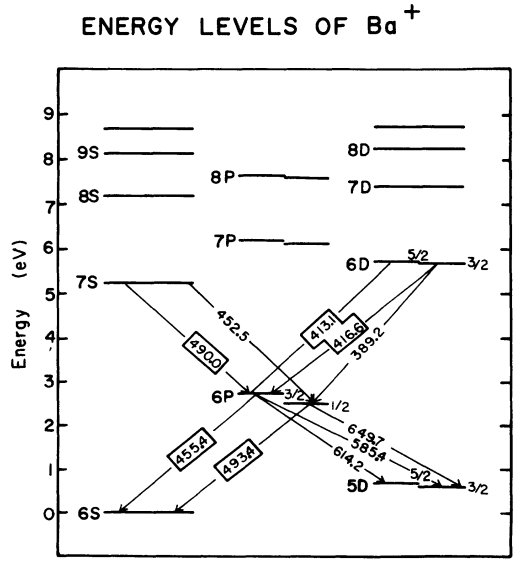

FIG. 1. Energy-level diagram of Ba^+. The boxed-in wavelengths (in nm) indicate the emissions observed in the present study.

A. Electron source

The magnetically confined electron source and tests for spiralling of the electrons have been described in detail.[9,17,18] The use of the source for excitation of Ca^+ and associated systematic errors have also been discussed, including energy calibration and measurement of energy spread. Magnetic field confinement of the beam is of considerable benefit for producing sufficient electron density to obtain measurable signal at low electron energies.

For the present Ba^+ study the temperature of the cathode was reduced somewhat compared to the Ca^+ work. This reduction compensated for the background light from the cathode which was greater at the Ba^+ wavelengths (455.5 and 493.4 nm) than for the Ca^+ wavelengths (393.4 and 396.9 nm). The temperature reduction was accompanied by a reduction in current and a decrease in width of the electron-energy distribution. Assuming the cross sections are finite at threshold, the electron-energy distribution at threshold energy is obtained by differentiating the onset curve. The full width at half maximum (FWHM) for the mea-

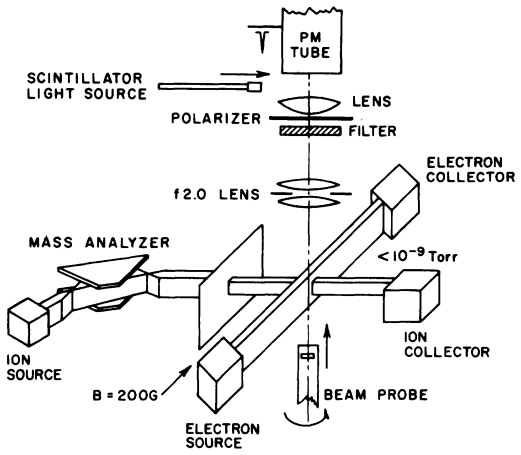

FIG. 2. Schematic of the apparatus.

surements reported here was 0.27 ±0.05 eV at $V_e = 2.7$ eV and a current $I_e = 7$ μA, and varied according to $\Delta V_e = 0.18 + 0.021 I_e / V_e^{1/2}$.

The reduction in current was not a severe problem to signal-intensity levels, but it did degrade the smoothness of the vertical distribution of the electron beam, $G(z)$. The electron source was still space-charge limited near threshold, but became emission-limited by about 100 eV primary energy. As conditions approach the emission-limited case, the vertical distribution of electrons reveals increasing structure associated with "hot spots" on the oxide cathode surface. This structure results in form factors which are more sensitive to slight changes in ion-beam vertical position and shape during data collection. (The electron-beam shape was degraded but still very stable with time.) Thus, contribution to the random uncertainty due to fluctuations in the form factor during data collection increased slightly.

The reduction in energy spread at the cathode might reasonably be expected to reduce spiralling of the electrons in the magnetic field, since thermal energy transverse to the field is reduced. The same path-length correction has been applied to the present data as was developed for the Ca^+ measurements, even though the reduction in cathode temperature is expected to reduce the path length by 1% at 2.7 eV (declining to 0.25% by 10 eV).

One small, but significant, modification was made to the electron gun which reduced the apparent number of secondary electrons in the collision region, and the associated uncertainty in the measured cross section. Vertical shear of the beam caused by space charge had extended the beam so that the upper and lower extremes were striking a slit edge prior to the collector, and secondaries were emitted from this electrode. The slit was elongated, and the number of secondaries, observed as current to other electrodes, was reduced; so that the uncertainty in cross sections due to secondaries is now believed to be less than 1%, even at the highest energy (750 eV) studied.

B. Ion beam

The hot-surface-ionization ion source was operated as previously described, except with a Ba charge. However, since the creation of metastable ions at the surface is of intrinsic interest and basic importance in deducing cross sections for excitation from the metastable levels, more details of the geometry and operation will be presented here.

The two major electrodes of the source, the emitter and the extractor, are machined from solid molybdenum in the shape of cylindrically symmetric Pierce electrodes, 8.4-cm diam. The heated portion of the emitter is a 0.13-mm-thick by 19-mm-diam W disk with a 0.38-mm-thick by 6.35-mm-diam Ir disk spot welded in its center. The extractor is placed 28 mm from the emitter, and Ba atoms are directed onto the hot emitter disk through channels in the extractor. In normal operation the extractor is at a potential of −330 V relative to the emitter, so there are electric fields the order of 100 V/cm at the emitter surface.

The Ir disk is heated from behind by electron bombardment with about 250 W of power. The brightness temperature was measured with an optical pyrometer as a function of applied power and the typical operating temperature was deduced to be 2200(±40) °K.

An estimate of the fraction of ions produced in metastable $5\,^2D_{5/2}$ and $5\,^2D_{3/2}$ states relative to $6\,^2S_{1/2}$ ground-state ions, can be obtained from application of the Saha equation. This leads to

$$\frac{N_+^*}{N_+} = \frac{g^*}{g} \exp\left(\frac{-E^* + E}{kT}\right), \tag{4}$$

where $g = 2J + 1$ (statistical weights), T is the operating temperature, and $E = 5.210$ eV, $E^*(5\,^2D_{3/2}) = 5.814$ eV, and $E^*(5\,^2D_{5/2}) = 5.913$ eV are the state energies relative to ground-state Ba. This procedure predicts $N_+(5\,^2D_{3/2})/N_+(6\,^2S_{1/2}) = 0.082$ and $N_+(5\,^2D_{5/2})/N_+(6\,^2S_{1/2}) = 0.074$ for 2200 °K; so that 86.5% of the ions in the beam should be ground state ($6\,^2S_{1/2}$) and 13.5% should be metastables ($5\,^2D_{3/2} + 5\,^2D_{5/2}$). The assumption that the Saha relation will lead to the correct ratio of metastables at the hot surface has not been tested. Indeed, it is clear that strict equilibrium does not exist, but there is good reason to believe that there is local thermodynamic equilibrium,[19] making use of Eq. (4) valid. We will use the predicted ratio to estimate cross sections, but call attention to this uncertainty, the magnitude of which we cannot assess. It is expected that the metastable population is equal to or less than that given by Eq. (4).

With the hope of changing the metastable population of the beam, an attempt to vary the operating temperature was made. However, insufficient ions were produced at temperatures below 2150 °K, and it was found inconvenient to obtain temperatures above 2270 °K; therefore, no significant changes in metastable population were achieved.

C. Mass analysis

The 60° sector magnet provides only partial separation of the natural isotopes of Ba. Exami-

nation of intensity of transmitted ion current as a function of applied magnetic field together with the natural isotope abundances leads to estimated isotope fractions of 89% mass 138, 8.5% mass 137, and 2.4% mass 136 in the ion beam for data-collection conditions. Because mass 137 has nuclear spin $\frac{3}{2}$ while masses 138 and 136 have spin 0, the polarization of the emitted radiation will be characteristic of the isotope mixture given above.

D. Photon detection

Photons are collected by $f/2.0$ optics and after passing through an interference filter are converged to a slightly out of focus spot on the photomultiplier. A polarizer is inserted into the light path only for polarization measurements, and its measured polarizance,[20] $K=0.993$ at wavelength 420.2 nm, was used to correct all polarization measurements.

Except for filters, the photodetection system was unchanged from previous descriptions. The photomultiplier employed was new, but of the same model and characteristics previously described. The photomultiplier sensitivity (monitored by scintillator light source) decayed by about 20% in one year's time, rapidly at first, and then more slowly. From the time of calibration of the optical system until final data collection, the decay of sensitivity was about 10%. During this important latter period, the response of the photomultiplier to a small, stable, low-temperature tungsten lamp viewed through a monochromator at 455.4 nm showed the same decay (within ±1%) as the response to the scintillator monitor.

The filters used for observation of the resonance radiation (455.4 and 493.4 nm) had nominal FWHM of 10.0 nm, and each had transmission peaks which were flat (within a few percent of maximum) for about 5.0 nm. While such flat-topped filters are desirable for this application, the cascade emissions at 452.5 and 490.0 nm (see Fig. 1) are, unfortunately, also transmitted through the filters intended to isolate 455.4 and 493.4 nm, respectively.

The absolute transmissions of these filters at the resonance wavelengths were measured in a double monochromator setup. The relative transmissions as a function of wavelength were measured using a monochromatic light source which could be inserted into the collision volume and scanned in wavelength. Thus, the relative transmissions were measured with the filters in the apparatus at operating temperature and orientation. These measurements gave transmissions of 0.61 at 455.4 and 0.53 at 452.5 nm for the 455.4-nm filter, and 0.66 at 493.4 and 0.59 at 490.0 nm for the 493.4-nm filter. Since the filters are almost as transparent at 452.5 and 490.0 nm as at the resonance wavelengths, we expect to see this extra light leaking through the filters and contributing to the apparent emission cross section.

In a sense, the cascade transitions $7\,^2S_{1/2} \rightarrow 6\,^2P_{1/2}$ at 452.5 nm and $7\,^2S_{1/2} \rightarrow 6\,^2P_{3/2}$ at 490.0 nm contribute twice to the apparent cross sections—through "leakage" as described above, and through cascade population of the $6\,^2P_{1/2}$ and $6\,^2P_{3/2}$ levels. In order to subtract these effects, separate measurements were made of the 490.0-nm emission cross section; and from this the 452.5-nm emission could be estimated using expected relative intensities taken from Miles and Wiese.[21] The disentanglement of leakage and cascade contributions to cross sections is outlined in the Appendix.

The interference filter used for 490.0 nm has nominal FWHM 5.0 nm centered at 487.0 nm with transmission of 0.201 at 490.0 nm. In this case we must be concerned about "leakage" of the 493.4-nm radiation. Even though the transmission of the 490.0-nm filter at 493.4 nm is only 0.019, the "leakage" is substantial because of the much greater intensity of the 493.4-nm radiation.

To obtain further information on cascade we observed the radiation at 413.1 and 416.6 nm from $6\,^2D_{5/2} \rightarrow 6\,^2P_{3/2}$ and $6\,^2D_{3/2} \rightarrow 6\,^2P_{3/2}$, using a filter of nominal FWHM 10.0 nm centered at 415.8 nm with measured transmissions of 0.54 at 413.1 nm and 0.60 at 416.6 nm. In this case, the 389.2-nm emission can be estimated again using data from the tables of Miles and Wiese.[21]

The transmissions of these last two filters, isolating 490.0 nm and (413.1 +416.6) nm, were not measured *in situ* as were the resonance-line filters, but were measured with a spectrophotometer. The temperature of the filters in the crossed-beams apparatus was observed to be 12.8 °C lower than when these transmissions were measured. The passband of such filters shifts with temperature, nominally +0.01 nm/°C, and this shift, causes an appreciable correction and uncertainty to the transmission of the 490.0-nm filter. The transmission quoted above is after this correction is applied.

E. Optical calibration

Again, apparatus and procedures are unchanged from previous descriptions,[9,17] and will not be described in detail here. A monochromatic light source (which could be inserted into the collision volume) was compared to a standard of spectral radiance by viewing both sources with a radio-

meter consisting of a grating monochromator with lens preoptics, an interference filter for additional dispersion of scattered light, and a cooled photomultiplier. The monochromatic "transfer" light source was then inserted into the collision volume at height z_0; and $D(z_0, \lambda)$, defined above, was determined. The standard of spectral radiance used here was a low-temperature vacuum tungsten-strip lamp calibrated by the National Bureau of Standards[22] by direct comparison to the gold point black-body standard at several wavelengths including 455.4 and 493.4 nm.[23] The calibrated strip lamp was used for a single careful calibration of the spectroradiometer. The calibrated spectroradiometer then was used to view the transfer light source, and the transfer to the crossed-beams apparatus was executed. The transfer was repeated about 10 times at each of the 5 wavelengths, 455.4 nm (Ba^+), 493.4 nm (Ba^+), 396.8 nm (Ca^+), 393.4 nm (Ca^+), and 391.4 nm (N_2^+), in order to obtain statistics on the transfer process.

Only the first two of the calibration wavelengths are directly applicable to the present work, but all were employed in interpolating to intermediate wavelengths. The interpolation was done by dividing out the filter transmissions from the measured sensitivity. A smooth curve was drawn between these points, which was taken to represent the sensitivity without filter at all included wavelengths. The sensitivities, $D(z_0, \lambda)$, at 490.0, 416.6, and 413.1 nm were obtained by reading values from the curve and multiplying by the appropriate filter transmissions. Of course, the accuracy is poorer than at the primary wavelengths.

Measured values of $D(z_0, \lambda)$ were for 455.4 nm through 455.4 filter, 0.742×10^{-3} counts/photon;

TABLE I. Significant uncertainties associated with apparatus and absolute calibration (in percent).[a]

	3 eV		100 eV	
	Direct sum	Quadrature	Direct sum	Quadrature
Relative uncertainties				
Path-length correction	2.0		0.2	
Form factor	1.6	3.6	1.6	1.8
Uncollected currents—secondaries	0.2		0.5	
Scintillator use	1.0		1.0	
Horizontal ion-beam position	1.5		1.5	
Totals	6.3	4.0	5.0	2.4
Absolute uncertainties				
Ion velocity	0.2			
Electron-current measurement	1.0			
Ion-Current measurement	1.0			
Totals	2.2	1.5		
Absolute Optical Calibration				
NBS calibration of strip lamp	2.5	2.5		
Our use of strip lamp	5.1	2.1		
Radiometer	4.2	2.6	Quadrature total Uncertainty in $D(z_0, \lambda)$	
Transfer	7.2	3.4		
Totals	19.0	5.4		
Additional uncertainties in $D(z_0, \lambda)$				
455.4 nm through 455.4 nm filter	0	0	5.4	
493.4 nm through 493.4 nm filter	0	0	5.4	
452.5 nm through 455.4 nm filter	3.5	2.6	6.0	
490.0 nm through 493.4 nm filter	3.5	2.6	6.0	
490.0 nm through 487.0 nm filter	19.5	10.1	11.5	
493.4 nm through 487.0 nm filter	22.0	14.3	15.3	
413.1+416.6 nm through 415.8 nm filter	7.0	4.0	6.8	

[a] An attempt has been made to take values roughly equivalent to the statistical 98% C. L. (~3 SD). Both linear and quadrature combinations are shown. When uncertainties have a possible correlation, they are first added linearly, and then in quadrature with remaining uncertainties.

493.4 nm through 493.4 filter, 0.649×10^{-3} counts/photon; 452.5 nm through 455.4 filter, 0.653×10^{-3} counts/photon; 490.0 nm through 493.4 filter, 0.596×10^{-3} counts/photon; 490.0 nm through 487.0 filter, 0.203×10^{-3} counts/photon; 493.4 nm through 487.0 filter, 0.019×10^{-3} counts/photon; and 413.1 +416.6 nm through 415.8 filter, 0.783×10^{-3} counts/photon.

F. Systematic uncertainties

Estimated systematic uncertainties associated with the measurements are listed in Table I. An effort has been made to assess these uncertainties at what we shall call a "high confidence level" which we feel is comparable to the 98% confidence level applied to statistical uncertainties. Individual uncertainties can be added linearly, or combined in quadrature. Both combinations are shown, except that in the quadrature case, if separate uncertainties are judged to have a possible correlation, they are added linearly with each other and then in quadrature with others not correlated.

The uncertainty in the strip-lamp calibration by NBS[22] is primarily in the thermodynamic temperature of the gold point. The uncertainty in our use of the strip lamp includes considerations of alignment, current accuracy and stability, possible change with use, and solid angle of observation. The radiometer uncertainty includes uncertainty in evaluation of radiometric integrals[9,17] as well as possible changes of radiometer sensitivity. The transfer uncertainty includes consideration of systematic uncertainty associated with light-source construction and use as well as statistics of the repeated transfers. The additional uncertainties at 490.0 nm and (413.1 +416.6) nm, where direct calibration is not executed, include uncertainty in interpolation between primary calibration points and uncertainty of transmission of filters as used in the crossed-beam apparatus (discussed in Sec. II D). Other uncertainties in cross sections associated with statistics of data, anistropy of radiation (Y_Ω), metastables, and light leakage through filters have not been listed in Table I. The quadrature combinations will be used in final assessment of cross-section uncertainties with the qualification regarding correlated uncertainties noted above.

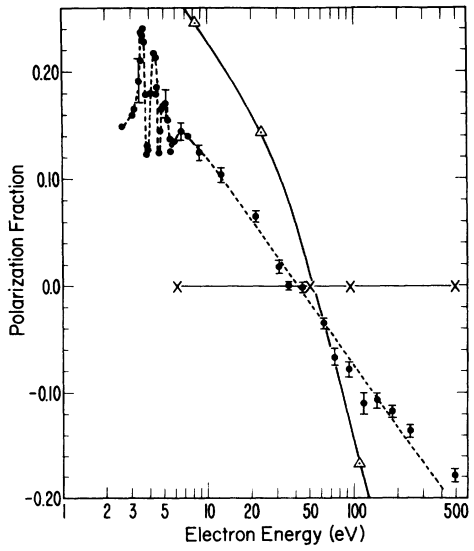

FIG. 3. Observed polarization fractions vs electron-impact energy: ●—polarization of 455.4-nm radiation ($6\,^2P_{3/2}\rightarrow 6\,^2S_{1/2}$); ×—polarization of 493.4-nm radiation ($6\,^2P_{1/2}\rightarrow 6\,^2S_{1/2}$); △—polarization of the mixture of 413.1-nm radiation ($6\,^2D_{5/2}\rightarrow 6\,^2P_{3/2}$) with 416.6-nm radiation ($6\,^2D_{3/2}\rightarrow 6\,^2P_{3/2}$). Bars shown are one standard deviation added to the uncertainty due to path-length correction.

III. RESULTS

A. Polarization

The linear polarizations of the emissions at 455.4, 493.4, and (413.1 +416.6) nm are presented in Fig. 3 as a function of impact energy. The polarization fraction has been evaluated as $P=(I_\parallel - I_\perp)/(I_\parallel + I_\perp)$ where $I_\parallel$ is the radiation intensity with the polarizer axis parallel to the electron axis, and $I_\perp$ is with polarizer axis perpendicular. The results are presented after small corrections are applied for polarizance of the polarizer, finite solid angle, electron path length,

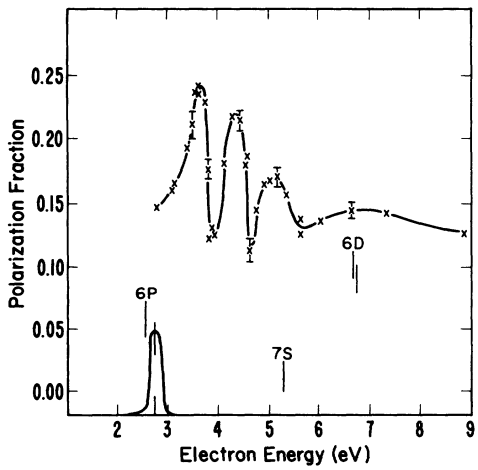

FIG. 4. Polarization fraction near threshold for 455.4-nm radiation ($6\,^2P_{3/2}\rightarrow 6\,^2S_{1/2}$). Positions of energy levels of Ba^+ are shown, and the electron-energy distribution is illustrated at threshold for excitation of $6\,^2P_{3/2}$. Bars represent one standard deviation.

and smearing due to spiralling trajectories (see Ref. 9 for details). These observations of the linear polarization of observed emissions may contain a small contribution from excitation of metastables in the ion beam and from cascade.

Since the ion is sufficiently slow to be considered stationary during the collision and subsequent emission, the experiment identifies only the electron-beam axis, and has symmetry about it. The only significant effect of the magnetic field is slight smearing of the direction of this axis due to spiralling trajectories of the electrons in the field, and a small correction has been applied for this. Thus, the analysis of Percival and Seaton[24] and of Flower and Seaton[25] expressing polarization in terms of partial cross sections (σ_m) for populating magnetic sublevels (m_L) should apply in the present case. The expected high-energy behavior of the σ_m cross sections can be used to predict the infinite-energy polarization. However, unlike electron-atom excitation, a simple prediction of polarization at threshold cannot be made for ion excitation because of the Coulomb interaction.

The polarization of the 493.4-nm radiation from the $6\,^2P_{1/2} \rightarrow 6\,^2S_{1/2}$ is expected to be zero.[24,26] The four measurements (Fig. 3) confirm this expectation. On the same basis, the 490.0-nm radiation has been assumed to be unpolarized. The radiation from the two lines 413.1 and 416.6 nm from the $6\,^2D_{5/2} \rightarrow 6\,^2P_{3/2}$ and $6\,^2D_{3/2} \rightarrow 6\,^2P_{3/2}$ transitions might be expected to be strongly polarized, and three measurements were made despite low signal levels and long data-collection times. As shown in Fig. 3, the polarization fraction is larger and has a steeper slope than the 455.4-nm case.

Detailed measurements of the polarization of the 455.4-nm radiation from $6\,^2P_{3/2} \rightarrow 6\,^2S_{1/2}$ were made and are shown in Figs. 3 and 4. The behavior of the polarization with increasing impact energy is approximately as expected on the basis of the Percival and Seaton treatment. The predicted infinite-energy polarization is −0.401 for our nuclear isotope mixture.

Polarization of impact-excited radiation has recently been discussed in the context of more general formalism by Fano and Macek.[26] Qualitatively, their treatment connects the momentum transfer from electron to target with the collision-produced alignment of the excited target. At threshold the momentum transfer should be along the electron direction and at high energy should be dominantly transverse to the electron direction of motion. The corresponding polarization of emitted radiation should be positive near threshold and proceed to negative polarization at high energies. The polaization is expected to change sign at about 10 times threshold energy. This view (not different from previous result of Percival and Seaton) describes the present measurements remarkably well, except for the structure near threshold.

Near threshold the polarization of the 455.4-nm radiation exhibits strong structure which is shown in greater detail in Fig. 4. This structure cannot be associated with excited states of the ion, which are placed on the figure at their respective energies. Fano and Macek[26] mention this structure in terms of strong correlation between the impact electron and the excited-target electron. If the correlation is of sufficient duration, $> 10^{-14}$ sec, extensive exchange of angular momentum may occur between the electrons, resulting in reduction of the target alignment and hence of the polarization of subsequent emission. In the present case such correlation of the electrons might be associated with autoionizing states of the Ba atom. The existence of such states with configuration $6pnl$ and $5dnl$, lying just below the $6P$ and $5D$ ionic levels, has been demonstrated by ultraviolet absorption studies.[27–29] The autoionizing levels involved here should have configurations $6dnl$ or $7snl$ and have not previously been observed.

The finite-energy spread of our electron beam (shown schematically at threshold in Fig. 4) precludes determination of the natural widths of these features, and the natural maxima and minima may be much higher and lower than shown. The electron-energy distribution may in fact overlap more than one autoionizing state. Thus, no additional analysis of these features is attempted here. The minima are located at approximately 3.9, 4.6, and 5.7 eV.

The polarization of 393.4-nm radiation from the analogous $4\,^2P_{3/2}$-$4\,^2S_{1/2}$ transition in Ca^+ did not exhibit structure.[9] However, there was no effort to search for structure, and the data were not taken with close enough energy spacing to define oscillations of the type seen for Ba^+.

Structure has been observed in polarization of emission from atoms. For example, the 388.9-nm emission of He exhibits a sharp minimum within a few volts of threshold (see review of Fano and Macek[26] for discussion). The recently observed polarization of Ca resonance line 422.7 nm[30] also exhibits a sharp dip followed by additional structure just above threshold, but the additional structure may be influenced by cascade so that interpretation does not clearly rely on resonances. In the case of Na, recent calculations[31] clearly indicate small structure in the polarization of the D lines near threshold associated with resonances, and some structure has been observed.[32]

B. Cross sections

The apparent emission cross sections, defined by Eq. (1), for the 455.4-nm radiation and for the (413.1 +416.6)-nm radiation are shown on Fig. 5. The data were collected over a period of several months. Usually the electron energy was stepped through a set sequence controlled automatically, and the sequence was repeated for up to 16 h. Each data point represents the average of the repeated trials of a particular energy during such a data run. At electron energy about 4 eV, for 455.4-nm radiation, the signal-plus-noise rate was about 13 counts/sec, with noise accounting for about 3 counts/sec. The statistical precision of data points is not constant, but where feasible, data collection was continued until the total counts at a particular energy represented about 1% counting statistics (for 455.4- and 493.4-nm cases).

The electron-energy scale was calibrated by observation of onset of helium emissions (see Ref. 9), without any input from observation of the Ba^+ or Ca^+ thresholds. The thresholds observed for Ba^+ are within 0.1 eV of the expected values. There exists the possibility of small changes in contact potential which could contribute to scatter in the data since adjacent data points may be separated by a month or more in time. A small number of the data points were obtained without chopping the electron beam, and in this case the energy scale is not as well established.

Included in the apparent cross sections such as shown in Fig. 5, are contributions from several sources which must be subtracted to obtain either line-emission cross sections or level-excitation cross sections. First, as discussed in Sec. II B, probably 13.5% of the target-ion beam is in the $5\,^2D_{3/2+5/2}$ metastable level. Contributions from this source show up as below-threshold-energy "shoulders" in the data of Fig. 5. Second, light from the $7\,^2S_{1/2}$-$6\,^2P$ transitions leaks through the filters used for observing the resonance lines, as noted in Sec. II D. If one subtracts these two contributions, the line-emission cross section for excitation from the ground state will result. To obtain level-excitation cross sections, one must subtract the cross section for cascade population of the level, and correct the cross section for the fact that the level branches in its decay, e.g. the $6\,^2P_{3/2}$ level may decay to the $6\,^2S_{1/2}$, the $5\,^2D_{3/2}$, or the $5\,^2D_{5/2}$ levels. Subtraction of the metastable contribution involves the assumption that the shape of the cross section for excitation from the metastable level is the same as that from the ground state. This and other details of the data analysis are discussed in the Appendix.

Line-emission cross sections and level-excitation cross sections are tabulated in Table II. Figures 6–9 show level-excitation cross sections for excitation of the $6\,^2P_{3/2}$, $6\,^2P_{1/2}$, $6\,^2D_{3/2+5/2}$, and $7\,^2S_{1/2}$, respectively. Values shown for the cross section at threshold were in each case obtained by a simple straight-line extrapolation through the group of measurements nearest threshold energy. Of course, an additional uncertainty is included in Table II for this extrapolation. The excitation cross sections for $6\,^2S_{1/2} \rightarrow 6\,^2D_{3/2+5/2}$ and $6\,^2S_{1/2} \rightarrow 7\,^2S_{1/2}$ are obtained from the (413.1 +416.6)-nm and 490.0-nm emissions and estimates based on the relative transition probabilities. The metastable contributions are subtracted, but cascade from higher levels, particularly $7\,^2P$ and $8\,^2P$, may be present in these cases.

The uncertainties presented in Table II include the quadrature sum of the statistical uncertainty (at 98% confidence level), all of the uncertainties associated with apparatus and optical calibration from Table I, and the uncertainties associated with each subtraction (see Appendix). We note again that no uncertainty has been allowed for possible error in estimating the state composition of the incident beam.

Finally, the magnitudes of the below-threshold shoulders on each observed emission together with the estimated fraction of the beam in the metastable states allow estimates of the cross sections at threshold for excitation from the two $5\,^2D_{3/2+5/2}$ states to each level; $6\,^2P_{1/2}$, $6\,^2P_{3/2}$, $7\,^2S_{1/2}$, and $6\,^2D_{3/2+5/2}$. These estimates are presented in

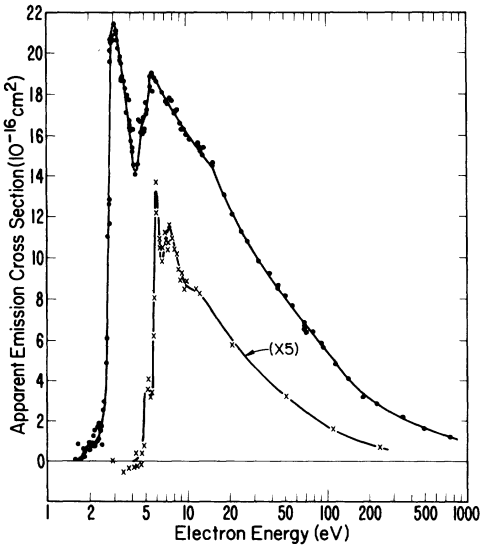

FIG. 5. Apparent emission cross sections vs electron energy for 455.4-nm (•-•-•) and 5 times the cross section for (413.1 + 416.6) nm (×-×-×). These are observed emissions before any attempt to correct for light "leakage" or the presence of metastable ions in the beam.

Table III. Note that a relatively large error in the estimated incident-beam state population has a small effect on the cross sections for excitation from $6\,^2S_{1/2}$ but has a much larger effect on these threshold estimates of cross sections for excitation out of the $5\,^2D$ states. An example is discussed in Sec. IV.

IV. DISCUSSION

A. General shape of cross sections

All of the cross sections, Figs. 6–9, have similar shape: a sharp peak at threshold followed by a second peak, a distinct break in slope, and smooth high-energy behavior. In the case of $6\,^2S_{1/2} \rightarrow 7\,^2S_{1/2}$ excitation, extracted from the 490.0-nm emission and shown in Fig. 9, the second peak is not outside of the high-confidence relative uncertainty estimates.

For the $6\,^2S_{1/2} \rightarrow 6\,^2P_{3/2}$ and the $6\,^2S_{1/2} \rightarrow 6\,^2P_{1/2}$ excitations the structure is definite, even after removal of cascades and light leakage. In addition to the two peaks and slope break which are readily identified in the $6\,^2S_{1/2} \rightarrow 6\,^2P_{3/2}$ and $6\,^2S_{1/2} \rightarrow 6\,^2P_{1/2}$ excitations (Figs. 6 and 7), there appear small features at energies above the second peak which

TABLE II. Absolute line-emission and level-excitation cross sections for electron-impact excitation of Ba^+ in the $6\,^2S_{1/2}$ ground state.[a]

Energy	Emission		Excitation	
(eV)	493.4 nm	455.4 nm	$6\,^2P_{1/2}$	$6\,^2P_{3/2}$
2.51	14.7*		20.0*(10)	
2.72		25.7*		34.7*(10)
3.0	13.3(8)	23.8(9)	18.1(9)	32.2(9)
3.6	11.2	19.9	15.3	26.9
4.0	9.6	17.4(11)	13.2	23.5
4.6	8.8(12)	16.8	12.0(13)	22.7(12)
5.0	9.0	16.9	12.2	22.9
5.6	10.1(11)	18.2(10)	11.7	21.2
6.0	9.3	17.7	9.7	18.6
7.0	8.9	17.1	9.5	18.6
8.0	9.1	17.1	10.2	19.2
10.0	9.0	16.3	10.6	18.9
14.0	7.9(8)	15.2(8)	9.5(14)	18.2(10)
20.0	6.5	12.7	7.8	15.2
30.0	5.5	10.3	6.7	12.5
50	4.2	8.4	4.7	10.4
70	3.6(7)	7.2(7)	4.4(10)	8.8(8)
100	2.9	5.7	3.5	7.2
142	2.30	4.4	2.9	5.5
237	1.69(7)	3.11(7)	2.2(8)	4.0(8)
345	1.26	2.34	1.67	3.0
495	0.94	1.75	1.26	2.31
747	0.62	1.28	0.84	1.71
	490.0 nm	413.1 + 416.6 nm	$7\,^2S_{1/2}$	$6\,^2D_{3/2+5/2}$
5.25	3.40*		5.4*(30)	
5.72		2.81*		4.3*(22)
6.0	2.83	2.44	4.5(29)	3.7(19)
6.5	2.49	1.86	4.0(33)	2.8
7.0	2.57	1.91	4.1	2.9
8.6	1.70	1.78	2.7	2.7
12.0	1.04	1.51	1.6	2.3
21.4	0.80	1.04	1.3(37)	1.6(19)
70.0	0.33	0.51	0.54	0.77
105	0.27	0.28	0.42(38)	0.43
237	0.13	0.13	0.20(42)	0.20(18)
747	0.0		0.0	

[a] Units are 10^{-16} cm^2. Representative total uncertainties in % are shown in parentheses; and are the quadrature combination of random and systematic uncertainties, both taken at what is judged to be equivalent to the 98% confidence level. Values marked with an asterisk (*) are threshold values obtained by graphical interpolation.

are not definite. *These wiggles are much smaller than relative uncertainties* and may be a product of the data analysis procedure, or $7\,^2P$ and $8\,^2P$ cascade; they probably deserve little attention.

At high energies the cross sections are smooth and fall off much as anticipated. The $6\,^2S \rightarrow 6\,^2P$ excitations are optically allowed and are expected to fall off as $(\log E)/E$ (see Fig. 10). The $6\,^2S \rightarrow 6\,^2D$ and $6\,^2S \rightarrow 7\,^2S$ excitations are optically forbidden and are expected to fall off as $1/E$.[33]

The cascade contributions from $7\,^2S_{1/2}$ and $6\,^2D_{5/2 \text{ and } 3/2}$ are significant in this work, and certainly larger than in the corresponding Ca^+ case where the thresholds for $5\,^2S_{1/2}$ and $4\,^2D_{5/2 \text{ and } 3/2}$ cascade to $4\,^2P$ levels are not discernable in the emission from the $4\,^2P$ states. In atomic systems the relative cascade in He and in Hg (both two-electron systems) is compared in the review by Moiseiwitsch and Smith.[34] In assessing the possible cascade contributions from levels higher than $7S$ and $6D$, we note the isoelectronic case of Cs. Here Zapesochnyi and Shimon[35] measure the total cascade contribution

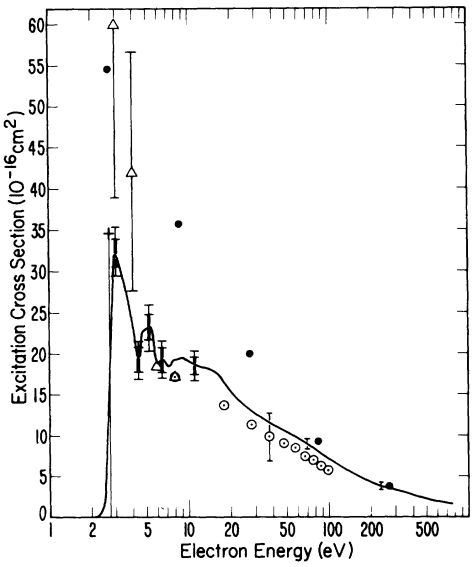

FIG. 6. Electron-impact excitation cross section vs electron energy for the $6\,^2S_{1/2} \rightarrow 6\,^2P_{3/2}$ excitation of Ba^+. Present data—solid line, the extrapolated threshold value indicated by +; data of Bacon and Hooper (Ref. 7)—0; data of Pace and Hooper (Ref. 8)—△; Coulomb-distorted-wave calculation of Burgess and Sheorey (Ref. 15)—●. Bacon and Hooper's data are normalized to Pace and Hooper's data at 8 eV; and both have been corrected for leakage, cascade, and metastables as discussed in the text. Bars represent the quadrature combination of high confidence (defined in text) systematic uncertainties together with random uncertainties at 98% C. L. The inner bars on present data represent high confidence *relative* uncertainties.

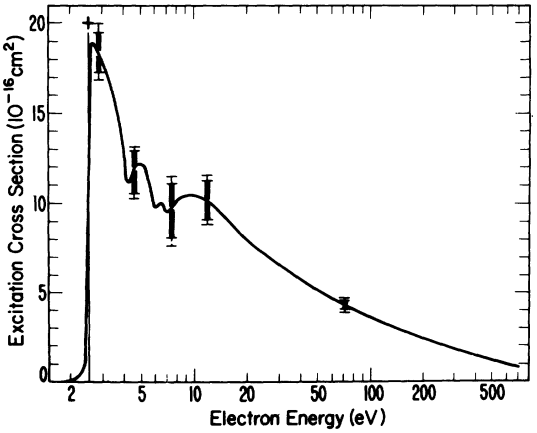

FIG. 7. Electron-impact excitation cross sections vs electron energy for $6\,^2S_{1/2} \rightarrow 6\,^2P_{1/2}$ of Ba^+—solid line, with extrapolated threshold value given by +. Inner error bars are high confidence relative uncertainties and outer error bars are high confidence total uncertainties.

in populating the $6\,^2P_{3/2}$ level from nS and nD levels greater than $7S$ and $6D$ up to $n = 14$, and find 5.6% if contributions are added at their peaks. Away from their peaks the total contribution is apt to be smaller.

In considering the structure in the excitation cross sections—particularly those shown in Figs. 6 and 7—one notes that the first deep minimum and peak occur below the 5.25-eV threshold for $7S$ excitation. Even though small corrections have

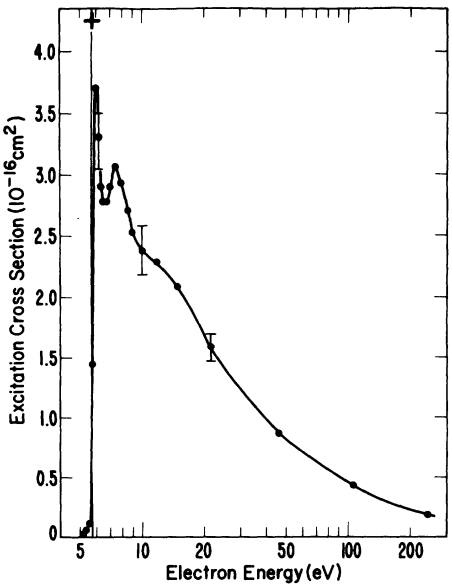

FIG. 8. Electron-impact excitation cross section for $6\,^2S_{1/2} \rightarrow 6\,^2D_{3/2+5/2}$ of Ba^+ vs electron energy. Bars are high confidence *relative* uncertainties.

been made for excitation of cascade levels from the $5D$ states, it is clear that errors in cascade assessment are not the cause of the structure, and one must look to physical processes operative in the $6\,^2P_{3/2}$ and $6\,^2P_{1/2}$ excitations. The features might be attributed to the resonances here referred to as autoionizing states of the Ba atom having configuration $7snl$ and $6dnl$, which we invoked to explain the structure in the 455.4-nm polarization. Even though the polarization structures appearing at 3.9, 4.6, and 5.7 eV, are not directly correlated in energy with the structures in the cross section, the autoionizing levels are good candidates for the cause of the structure. The Ca^+ excitation of $4\,^2S_{1/2}$-$4\,^2P_{3/2}$ also showed structure at energies where such autoionizing levels of the Ca atom could appear.[9] The Ba autoionizing levels would appear to be stronger (at least in their effect on Ba^+ emissions and polarization) than for the corresponding Ca^+ case.

Of course, structure in excitation cross sections due to compound-state resonances is not new. A recent review by Schulz[36] in electron impact on atoms is available, so that no attempt to cite the many examples will be made here. Certainly the present results are an interesting addition, since they are for excitation of an ion, and since cascade contributions have been separated out to reasonable confidence.

Simply from statistical weights the ratio of excitations $6\,^2S \rightarrow 6\,^2P_{3/2}$ to $6\,^2S \rightarrow 6\,^2P_{1/2}$ might be expected to be 2 to 1. The present data exhibit deviation from this ratio at threshold (2.7 eV) where it is observed to be 1.7 to 1, approaching 2 to 1 by 6 eV. The electronically similar Ca^+ case[9] gave 2 to 1 within experimental uncertainty at all energies.

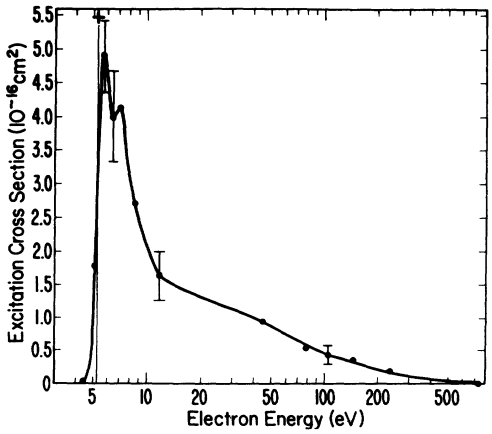

FIG. 9. Electron-impact excitation cross section for $6\,^2S_{1/2} \rightarrow 7\,^2S_{1/2}$ of Ba^+ vs electron energy. Bars are high confidence relative uncertainties.

TABLE III. Threshold cross sections for excitation from $5\,^2D_{3/2+5/2}$ state of Ba^+ to various levels.

Level	Electron energy (eV)	Estimated threshold excitation cross section (10^{-16} cm^2)	Estimated uncertainty[a] (%)
$6\,^2P_{3/2}$	2.0 eV	13.4	[a]±34%
$6\,^2P_{1/2}$	1.8 eV	9.8	±28%
$7\,^2S_{1/2}$	4.6 eV	7.4	±100%
$6\,^2D_{5/2+3/2}$	5.0 eV	6.9	±27%

[a] Additional uncertainty may result from uncertainty in level population of target ion beam (see text).

B. Comparison to other work

The work of Pace and Hooper[8] together with previous results of Bacon and Hooper[7] are presented as excitation cross sections for $6\,^2S_{1/2}$-$6\,^2P_{3/2}$ in Fig. 6 with the present results. Experimental aspects of their investigation are similar to the present work. The most notable differences are in the electron sources and optical calibration procedures. The magnetically confined electron source used here, with much higher electron densities, particularly at low energy, affords the present work significantly better precision. The higher signal allows investigation of the meta-

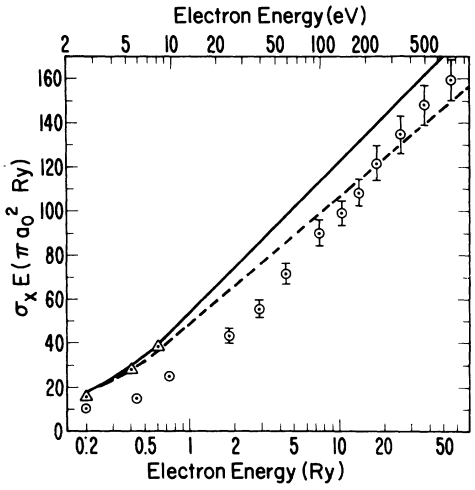

FIG. 10. Comparison of theoretical and experimental collision strengths for the Ba^+ $6s$-$6p$ transition. Present data—○; Coulomb distorted-wave calculations of Burgess and Sheorey (Ref. 15), with wave functions giving experimental oscillator strengths—dashed line, and with wave functions giving correct energy levels—solid line; Coulomb-Born II calculation of Petrini (Ref. 16)—△. Bars are quadrature combinations of high-confidence uncertainty in the excitation cross sections of $6\,^2S_{1/2} \rightarrow 6\,^2P_{3/2}$ and $6\,^2S_{1/2} \rightarrow 6\,^2P_{1/2}$ which are added for the $6s$-$6p$ transition.

stables, structure in cross section and polarization, and cascade contributions discussed above. The corrections applied to the apparent emissions, to obtain excitation cross sections almost certainly apply to the Pace and Hooper, and the Bacon and Hooper work as well. For presentation in Fig. 6, their data have been corrected in the same way as the present results. That is, subtractions from their reported emission cross sections have been made for light leakage, metastables, and cascades. To subtract leakage, it was assumed that their filter (5.0-nm-FWHM) transmitted 452.5-nm radiation at 0.50 times the transmission of the 455.4-nm resonance line. For their ion source, the ratios of metastables to ground-state ions produced were taken to be 0.07 for $N_+(5\,^2D_{3/2})/N_+(6\,^2S_{1/2})$ and 0.06 for $N_+(5\,^2D_{5/2})/N_+(6\,^2S_{1/2})$; so that 11% of the total beam is taken to be in the metastable states.

The agreement in magnitude of these two absolute measurements is well within the combined uncertainties of the experiments, except for the 3 and 4 eV points of Pace and Hooper. Pace and Hooper give ±23% uncertainty for the quadrature combination of uncertainties in the absolute optical calibration, and a linear sum of these quantities of 61%. Random uncertainties are about 25% for Pace and Hooper's work (3, 4, 6, and 8 eV) and about 10% for Bacon and Hooper's results (8 to 98 eV). Other systematic uncertainties in their experiments besides optical calibration are given as around 10%. The calibrated point at 8 eV of Pace and Hooper was used by them to normalize the results of Bacon and Hooper at this overlapping energy of their data. One could only conjecture as to the reasons why Pace and Hooper's data at 3 and 4 eV do not agree with the present measurements. We note only that the 3 and 4 eV points of Pace and Hooper were taken with low signal levels and have a large uncertainty associated with them; and that the discrepancy cannot be attributed to differing resolution of one or more sharp peaks in the cross section, since the electron-energy spread (approximately 0.3 eV) is about the same for the two experiments.

Also shown on Fig. 6 are calculations of Burgess and Sheorey[15] based on the Coulomb distorted-wave approach. The calculated result is significantly higher than the present results at threshold, as is anticipated. They are, however, below the divergent points of Pace and Hooper discussed above. As expected, the calculations converge to the measurements at high energy, and do so in a way very similar to the Ca^+ case.

Comparison at high energies of the calculation and experiment is more clearly shown in Fig. 10 by a plot of cross section times energy versus logarithm of energy. The theoretical high-energy limit of such a plot is a straight line with slope proportional to the optical oscillator strength of the transition. Two different calculations of Burgess and Sheorey[15] are shown. The upper curve used bound-state wave functions leading to correct bound-state energies. The lower curve used wave functions leading to the oscillator strength measured by Gallagher.[37] The experimental data lie below the theoretical curves until about 250 eV, about 100 times threshold energy. Considering the uncertainties on the experimental points, the data do not extend to high enough energies to clearly distinguish between these calculations. The Coulomb-Born (CB) II calculations of Petrini[16] at low energy are also shown in Fig. 10.

Barium plasmas have been used for basic plasma studies and development of diagnostic techniques. Hinnov *et al.*,[14] have measured rate coefficients for emission from the $6\,^2P$ levels of Ba^+ for use in such studies. A comparison of rate coefficients derived from the present work is therefore important and meaningful.

The rate of excitation of the $6\,^2P_{3/2}$ level of Ba^+ in a plasma is

$$\frac{dN(6\,^2P_{3/2})}{dt} = N(6\,^2S)N_e\alpha_S + N(5\,^2D_{3/2})N_e\alpha_{D_{3/2}} + N(5\,^2D_{5/2})N_e\alpha_{D_{5/2}}$$

$$= N(6\,^2S)N_e\left[\alpha_S + \frac{g(D_{3/2})}{g(S)}\exp\left(-\frac{(E_{D_{3/2}} - E_S)}{kT}\right)\alpha_{D_{3/2}} + \frac{g(D_{5/2})}{g(S)}\exp\left(-\frac{(E_{D_{5/2}} - E_S)}{kT}\right)\alpha_{D_{5/2}}\right] \equiv N(6\,^2S)N_e\bar{\alpha}, \tag{5}$$

where the last equivalence defines $\bar{\alpha}$, g's are statistical weights, N's are respective state densities, E's are state energies, and the rate coefficients (α's) are given in terms of the cross section for exciting the $6\,^2P_{3/2}$ level from the state J by

$$\alpha_J = \int_0^\infty \sigma_J(v)vf(v)\,dv\,. \tag{6}$$

Here $f(v)$ is the Maxwellian distribution of electron velocities v.

For cross sections of the type encountered here,

a good approximation to α_J is

$$\alpha_J = AT^{1/2}\Sigma_J(X_J+1)e^{-X_J}, \tag{7}$$

where A is a constant, T is electron temperature, Σ_J is the threshold value of σ_J, and $X_J = E_J/kT$. Using this, we can rewrite the expression for $\bar{\alpha}$,

$$\bar{\alpha} = \alpha_S\left[1 + \frac{g(D_{3/2})}{g(S)}\frac{\Sigma_{3/2}}{\Sigma_S}\frac{(X_{3/2}+1)}{(X_S+1)} + \frac{g(D_{5/2})}{g(S)}\frac{\Sigma_{5/2}}{\Sigma_S}\frac{(X_{5/2}+1)}{(X_S+1)}\right]. \tag{8}$$

Evaluation of α_S is done numerically using Eq. (6) and the measured excitation cross section for $6\,^2S_{1/2} \rightarrow 6\,^2P_{3/2}$. Cross sections, $\Sigma_{3/2}$ and $\Sigma_{5/2}$, are taken to be equal, each with a value one-half that of the total $5\,^2D_{3/2+5/2} \rightarrow 6\,^2P_{3/2}$ excitation given in Table III.

Figure 11 shows a comparison of $\bar{\alpha}$ thus deduced from present measurements, with $\bar{\alpha}$ measured by Hinnov *et al.*[14] The lined-in area representing Hinnov's data encompasses his estimated factor of 1.5 uncertainty in the value of $\bar{\alpha}$, as well as his uncertainties in temperature. The solid line represents our deduced value of $\bar{\alpha}$, and the dashed lines show the range of $\bar{\alpha}$ if cross sections change by amounts corresponding to the uncertainties in Tables II and III.

There is general agreement between the two sets of measurements within the stated uncertainties. However, Hinnov[38] believes there may be a true discrepancy present, and that it could arise from the metastable populations—either in his experiment or in ours. It is not appropriate for us to assess this in Hinnov's experiment, but we can examine effects in our own experiment of assuming a different metastable content in the beam than that deduced from equilibrium calculations. The dot-dashed curve in Fig. 11 shows $\bar{\alpha}$ calculated if one uses cross sections in Eqs. (6) and (8) resulting from assuming only 3.6% (rather than 13.5%) of the target Ba^+ beam is in the metastable $5D$ states. For this fraction we find the cross section at threshold for $6\,^2S_{1/2} \rightarrow 6\,^2P_{3/2}$ to be 31×10^{-16} cm^2 (a decrease of about 10% from Table II, Fig. 6) and $5\,^2D_{3/2+5/2} \rightarrow 6\,^2P_{3/2}$ to be 44×10^{-16} cm^2 (an increase of more than a factor of 3 from Table III).

The CB II results of Petrini[16] calculated at threshold (neglecting fine structure) give a ratio for excitation $6\,^2S_{1/2}$-$6\,^2P_{1/2+3/2}$ to $5\,^2D_{5/2+3/2} \rightarrow 6\,^2P_{1/2+3/2}$ of $\sigma_S/\sigma_D = 3.3$. Our results from Tables II and III give $\sigma_S/\sigma_D = 2.4 \pm 0.9$, in agreement with the calculated ratio. However, the results for matching our calculated $\bar{\alpha}$ to Hinnov (the dot-dashed curve discussed above) predict approximately $\sigma_S/\sigma_D = 0.7$, which is a factor 4.7 lower than calculated. The CB II calculations are not expected to give good results at threshold, but the ratios of cross sections should not be grossly incorrect. These observations lend support to the assumption of the calculated equilibrium beam populations with the attendant cross sections in Tables II and III, and the deduced $\bar{\alpha}$ given by the solid curve in Fig. 11.

Both Ba^+ and Ca^+ are alkalilike in structure—having a single S electron outside closed shells. Comparison of the S-$P_{3/2}$ resonance excitations reveals generally similar behavior with significant difference just above threshold. In each case, within the finite electron-energy spread, the cross section has a finite maximum value at the energy threshold for the process. In each case, there is a sharp decrease in the cross section to a minimum about 2 eV above threshold. In barium, however, this decrease is more pronounced, being about 40%, compared to about 7% in calcium. After the minima, the cross sections again rise to secondary maxima followed by normal declines—apparently going over into the expected $(1/E)\log E$ form at high energies. Both measurements meet the Coulomb-distorted-wave calculations of Sheorey and Burgess at about 250 eV, and agree with these calculations within experimental and theoretical uncertainties above this.

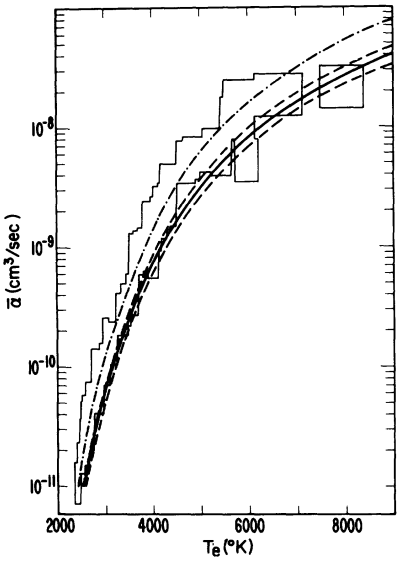

FIG. 11. Excitation rate for exciting the $6\,^2P_{3/2}$ level of Ba^+ as a function of electron temperature in a plasma. The lined-in area represents the data of Hinnov *et al.* (Ref. 14) encompassing quoted uncertainties; the solid line is deduced from the present data with dashed lines encompassing the absolute uncertainties listed in Table II; the dot-dashed line is deduced from the present data if the fraction of incident ions in metastable states is changed from the estimated 13.5% to 3.6%.

Neither cross section is accurately predicted by existing theory in the important threshold region.

In observations of various emissions from excitation of Ar II and Kr II, Zapesochnyĭ *et al.*[10,11] also observe a maximum near threshold followed by a second maximum 10 eV or so above threshold. The threshold behavior and subsequent structure are more difficult to assess in these cases, since the electron energy spread was several electron volts.

ACKNOWLEDGMENTS

We acknowledge helpful discussions with many colleagues, beyond those directly cited in the paper.

APPENDIX: EXTRACTION OF EMISSION CROSS SECTIONS FROM OBSERVED EMISSIONS

By employing four different interference filters, we have observed four "apparent" emission cross sections arising from electron impact on Ba^+. However, because of the presence of metastable ions in the incident beam, and because Ba^+ emissions of two different wavelengths are passed by three of the four filters used, these apparent emissions do not directly yield specific line emission cross sections (arising from electron impact on ground-state Ba^+) which we would like to measure.

In what follows we consider emission cross sections denoted by a subscript e and excitation cross sections denoted by subscript x. Furthermore, we use a second subscript b to denote excitation from our beam mixture of ground-state and metastable ions; the second subscript m denotes excitation from the metastable level; and the absence of a second subscript b or m implies excitation from the ground state. Thus, for example, $\sigma_{eb}(\lambda)$ is the emission cross section for wavelength λ when our target-beam mixture of states is bombarded; $\sigma_x(n^2L_J)$ is the excitation cross section of the level n^2L_J when ground-state ions are bombarded; and $\sigma_{xm}(n^2L_J)$ is the excitation cross section of the level n^2L_J when metastable ions are bombarded.

With any of the filters in place in the light-collection system, we observe a count rate or "signal." Equation (1) of the text relates an emission cross section to the measured quantities; but for three of the four filters used, there are two emission cross sections, $\sigma_{eb}(\lambda)$ and $\sigma_{eb}(\lambda')$, contributing to the count rate. A normalized signal S can be defined by Eq. (1) as the observed count rate normalized by all measured quantities and constants (integrated beam currents, form factor, anisotropy, etc.); except the absolute sensitivities, $D(z_0, \lambda)$ and $D(z_0, \lambda')$, which will be different for the two different wavelengths. Denoting such normalized signals S by subscripts H, S, K, and D for each of the four filters intended to isolate the 493.5 nm (H resonance line), 490.0 nm (from $7^2S_{1/2} \rightarrow 6^2P_{3/2}$), 455.4 nm ($K$ resonance line) and (413.1 +416.6) nm (from $6^2D_{5/2+3/2} \rightarrow 6^2P_{3/2}$), respectively, we can write

$$S_H = \sigma_{eb}(493.5)D_H(493.5) + \sigma_{eb}(490.0)D_H(490.0), \tag{A1}$$

$$S_S = \sigma_{eb}(490.0)D_S(490.0) + \sigma_{eb}(493.5)D_S(493.5), \tag{A2}$$

$$S_K = \sigma_{eb}(455.4)D_K(455.4) + \sigma_{eb}(452.5)D_K(452.5), \tag{A3}$$

$$S_D = \sigma_{eb}(413.1 + 416.6)\bar{D}_D(413.1 + 416.6); \tag{A4}$$

where the subscripts have also been used to distinguish the sensitivities $D(z_0, \lambda)$ for each of the four filters.

An additional relationship between $\sigma_{eb}(490.0)$ and $\sigma_{eb}(452.5)$ is obtained by recourse to relative transition probabilities given by Miles and Wiese.[21] Since these two emissions originate from the $7^2S_{1/2}$ level, they are simply related by the Einstein A values for decay to $6^2P_{3/2}$ and $6^2P_{1/2}$. Miles and Wiese give $A_{1/2}/A_{3/2} = 0.6$, with a conservative estimate of the uncertainty of ±50%. This then leads to

$$\sigma_{eb}(452.5) = 0.6\sigma_{eb}(490.0). \tag{A5}$$

There are now five equations, (A1)–(A5), in the five unknowns, and the system can readily be solved for the $\sigma_{eb}(\lambda)$. In Eqs. (A1)–(A3) the first term on the right-hand side represents the primary emission intended to be isolated by the filter in use, while the second represents the unwanted "leakage" light discussed in the text. Determination of each of the $D(\lambda)$'s is discussed in the text (Sec. II E) except for the quantity $\bar{D}_D(413.1 + 416.6)$ in Eq. (A4). We have chosen to represent the emission for the 413.1- and 416.6-nm lines originating from the $6^2D_{5/2}$ and $6^2D_{3/2}$ levels as a composite. The composite sensitivity has been obtained by further use of the tables of Miles and Wiese.[21] Assuming the $6^2D_{5/2}$ and $6^2D_{3/2}$ are collisionally populated according to statistical weights, and employing the relative transition probabilities, we anticipate that 0.909 of the composite light is 413.1 nm and 0.091 is 416.6 nm, so that,

$$\bar{D}_D(413.1 + 416.6) = 0.909D_D(413.1) + 0.091D_D(416.6). \tag{A6}$$

Since the two sensitivities on the right-hand side

TABLE IV. Sample of data analysis.[a]

Energy	Signal (10^{-19} cm^2× counts)	Subtract light leakage (10^{-19} cm^2× counts)	Emission cross section for our ion-state mix (10^{-16} cm^2)	Emission cross section for ground state ion (10^{-16} cm^2)	Cascades (10^{-16} cm^2)		Excitation cross section (10^{-16} cm^2)
455.4 nm	S_K	σ_{eb} (452.5)×D_K(452.5)	σ_{eb} (455.4)	σ_e (455.4)	σ_{eb} (490.0)	σ_{eb} (413.1 + 416.6)	$\sigma_X(6\,^2P_{3/2})$
3.0 eV	16.02(6.4)	0	21.60(6.4)	23.81(8.5)	0	0	32.2(9.0)
6.5	13.31(5.4)	0.89(54)	16.80(7.0)	18.35(9.0)	2.60(21.6)	2.00(10)	17.5(13.2)
70.0	5.01(3.2)	0.13(58)	6.58(3.7)	7.23(7.2)	0.36(30)	0.44(9.2)	8.5(8.2)
493.4 nm	S_H	σ_{eb} (490.0)×D_H(490.0)	σ_{eb} (493.4)	σ_e (493.4)	σ_{eb} (452.5)	σ_{eb} (389.2)	$\sigma_X(6\,^2P_{1/2})$
2.8 eV	7.85(5.7)	0	12.09(5.7)	13.28(8.1)	0	0	18.1(8.6)
6.5	7.12(5.1)	1.55(22)	8.58(9.1)	9.42(11.0)	1.56(55)	1.06(51)	8.7(20.3)
70.0	2.35(2.4)	0.21(28)	3.30(3.8)	3.61(7.3)	0.21(57)	0.22(51)	4.2(9.5)
490.0 nm	S_S	σ_{eb} (493.4)×D_S(493.4)	σ_{eb} (490.0)	σ_e (490.0)			$\sigma_X(7\,^2S_{1/2})$
6.5 eV	0.690(15.6)	0.163(23)	2.60(22.3)	2.48(26)			4.0(33)
70.0	0.133(11.9)	0.061(23)	0.35(30.0)	0.33(33)			0.54(38)
233.7	0.054(12.5)	0.027(23)	0.13(34.5)	0.12(37)			0.20(42)

[a]Quantities in parentheses are uncertainties in percent. The initial uncertainties are relative systematic errors from Table I added in quadrature with 98% C. L. random uncertainties. The σ_{eb} (λ) listed uncertainties do not include the ± 5.4% for absolute optical calibration. Final uncertainties are quadrature combinations of all "high confidence" estimates, given at each step in the table.

differ only by the transmission of the filter, 0.54 and 0.60, respectively, the composite sensitivity $\bar{D}_D$ is not sensitive to error in the multiplying factors, 0.909 and 0.091.

Level excitation cross sections

Our target beam consists of a fraction F of ground-state $6\,^2S$ ions, with the remainder being metastable $5\,^2D$ ions. The excitation from this beam mixture of a level n^2L_J can be written

$$\sigma_{xb}(n^2L_J) = F\sigma_x(n^2L_J) + (1-F)\sigma_{xm}(n^2L_J). \quad \text{(A7)}$$

The $\sigma_{xb}(n^2L_J)$ can be obtained from the $\sigma_{eb}(\lambda)$ of Eqs. (A1)–(A5) and appropriate branching ratios. In order to obtain $\sigma_x(n^2L_J)$ from Eq. (A7), then, we need $\sigma_{xm}(n^2L_J)$. Information allowing us to arrive at approximate values of these cross sections is contained in the apparent emission cross section curves such as shown in Fig. 5. At the lower energies of these curves one finds "shoulders" due to emission resulting from excitation of the metastables only. Using this near-threshold data, we define and measure a quantity

$$K = \sigma^b_{eb}(\lambda)/\sigma^a_{eb}(\lambda), \quad \text{(A8)}$$

where the superscript "b" delineates the emission cross section to be that above the threshold for excitation from the metastable state but below the threshold for excitation from the ground state; i.e., it specifies that $\sigma^b_{eb}(\lambda)$ is the value of the emission cross section on the "shoulder." The superscript a defines $\sigma^a_{eb}(\lambda)$ to be the observed emission cross section just above the threshold for excitation from the ground state. Now, recognizing that $\sigma^b_{eb}(\lambda)$ and $\sigma^a_{eb}(\lambda)$ are defined at energies where there is no cascade, and that the branching ratios are the same, we can rewrite Eq. (A8), in terms of excitation cross sections

$$K = \frac{\sigma_{xm}(n^2L_J)(1-F)}{\sigma_{xb}(n^2L_J)}. \quad \text{(A9)}$$

Here we have also made use of Eq. (A7) and the fact that by definition, $\sigma^b_x(n^2L_J) = 0$, in order to write the numerator in this form. We now make the reasonable approximation that $\sigma_{xm}(n^2L_J)$ and $\sigma_x(n^2L_J)$ have the same shape, so that Eq. (A9) will hold at all energies [making use also of Eq. (A7)]. Eliminating $\sigma_{xm}(n^2L_J)$ between Eqs. (A7) and (A8), we have for the cross section for excitation from the ground state

$$\sigma_x(n^2L_J) = \frac{1-K}{F}\,\sigma_{xb}(n^2L_J). \quad \text{(A10)}$$

This equation can be rewritten in terms of the emission cross sections resulting from the solution of Eqs. (A1)–(A5), giving

$$\sigma_x(n^2L_J) = \frac{1-K}{F}\left(\frac{\sum A_{rj}}{A_{rg}}\sigma_{eb}(\lambda_{rg}) - \sum_k \sigma_{eb}(\lambda_{kr})\right). \quad \text{(A11)}$$

Here A_{rj} are the Einstein A coefficients for transitions between a level r and lower levels j; λ_{rg} is the wavelength of emissions from r to the particular level g; λ_{kr} denote emissions from upper levels k which feed r by cascade. This expression is in suitable form for immediate evaluation of the cross sections for direct excitation out of the ground state of Ba^+ to the upper level of each of the four observed transitions. Specifically, from the onsets of the $\sigma_{eb}(493.5)$, $\sigma_{eb}(455.4)$, $\sigma_{eb}(490.0)$, and $\sigma_{eb}(413.1+416.6)$, we obtain values of K of 0.05 (±30%), 0.05(±30%), 0.17(±51%), and 0.22(±25%) for use in evaluating $\sigma_x(6\,^2P_{1/2})$, $\sigma_x(6\,^2P_{3/2})$, $\sigma_x(7\,^2S_{1/2})$, and $\sigma_x(6\,^2D_{5/2+3/2})$, respectively. The uncertainties in parentheses are "high confidence" as described in Sec. II and introduce uncertainty into the excitation cross sections of ±1.5%, ±1.5%, ±10%, and ±7% in the respective cases. Additional uncertainties of ±20% of the fractions K have been included to allow for the assumption in extending K to energies above threshold. The terms $\sum_j A_{rj}/A_{rg}$ are the branching ratios which have been measured by Gallagher[37] for the $6\,^2P_{1/2}$ and $6\,^2P_{3/2}$ resonance levels and are evaluated (less accurately) for the $7\,^2S_{1/2}$ and $6\,^2D_{5/2+3/2}$ excitations by further use of the tables of Miles and Wiese.[21] The branching ratios obtained are 1.361, 1.351, 1.60, and 1.515 in the respective cases. With the above evaluations, we write specifically from (A11) for energies above threshold.

$$\sigma_x(6\,^2P_{1/2}) = 1.495\sigma_{eb}(493.4) - 0.659\sigma_{eb}(490.0) - 0.566\sigma_{eb}(413.1+416.6), \quad \text{(A12)}$$

where the cascades $\sigma_{eb}(452.5)$ and $\sigma_{eb}(389.2)$ have been written in terms of $\sigma_{eb}(490.0)$ and $\sigma_{eb}(413.1+416.6)$ by use of Miles and Wiese's tables;

$$\sigma_x(6\,^2P_{3/2}) = 1.484\sigma_{eb}(455.4) - 1.098[\sigma_{eb}(490.0)+\sigma_{eb}(413.1+416.6)], \quad \text{(A13)}$$

where in both Eqs. (A12) and (A13) only the available cascade contributions from the $7\,^2S_{1/2}$ and $6\,^2D_{5/2+3/2}$ levels are accounted for. Further, we have within the approximation that cascade contributions are neglected

$$\sigma_x(7\,^2S_{1/2}) = 1.535\sigma_{eb}(490.0) \quad \text{(A14)}$$

and

$$\sigma_x(6\,^2D_{5/2+3/2}) = 1.366\sigma_{eb}(413.1+416.6). \quad \text{(A15)}$$

Expressions (A12)–(A15) have been used to obtain the excitation cross sections given in Table II and shown in Figs. 6–9.

Table IV presents actual numbers and uncertainties generated at three particular energies in the complete above analysis procedure. The case for S_D(413.1 +416.6) nm radiation, is more simply and directly analyzed and is not included in Table IV.

Finally, estimates of the threshold cross sections for excitations from $5\,^2D_{3/2+5/2}$ to each of $6\,^2P_{3/2}$, $6\,^2P_{1/2}$, $7\,^2S_{1/2}$, and $6\,^2D_{5/2+3/2}$ are made. The shoulders of the $\sigma_{eb}(\lambda)$ emission curves are taken to have arisen from excitations out of $5\,^2D$ states which are assumed to constitute 0.135 of the incident ions. Application of the appropriate branching ratios gives the threshold value of excitation cross sections immediately (given in Table III). So, for example, at threshold

$$\sigma_{xm}(6\,^2P_{3/2}) = (3.85/2.85)(1/0.135)\sigma_{eb}(455.4),$$

where determination of this cross section has averaged all data points of $\sigma_{eb}(455.4)$ within ±0.1 eV of 2.3 eV.

---

*Staff Member, National Bureau of Standards, Boulder, Colorado.

†This work was supported in part by the Controlled Thermonuclear Division of the U. S. Atomic Energy Commission.

[1]M. J. Seaton, in *Atomic and Molecular Processes*, edited by D. R. Bates (Academic, New York, 1962), p. 374.
[2]J. Cooper, Rep. Prog. Phys. 29, 35 (1966).
[3]M. F. A. Harrison, Br. J. Appl. Phys. 17, 371 (1966).
[4]K. T. Dolder, in *Case Studies in Atomic Collision Physics*, edited by E. W. McDaniel and M. R. C. McDowell (North-Holland, Amsterdam, 1969).
[5]G. H. Dunn, in *Atomic Physics*, edited by V. W. Hughes, V. W. Cohen, and F. M. J. Pichanick (Plenum, New York, 1969), p. 417.
[6]A. R. Lee and N. P. Carleton, Phys. Lett. A 27, 195 (1968).
[7]F. M. Bacon and J. W. Hooper, Phys. Rev. 178, 182 (1969).
[8]M. O. Pace and J. W. Hooper, Phys. Rev. A 7, 2033 (1973).
[9]P. O. Taylor and G. H. Dunn, Phys. Rev. A 8, 2304 (1973).
[10]I. P. Zapesochnyĭ, A. I. Imre, A. I. Daschenko, V. S. Vokstich, F. F. Danch, and V. A. Kel'man, Zh. Eksp. Teor. Fiz. 63, 2000 (1972) [Sov. Phys.—JETP 36, 1056 (1973)].
[11]A. I. Imre, A. I. Dashchenko, I. P. Zapesochnyĭ, and V. A. Kel'man, Zh. Eksp. Teor. Fiz. Pis. Red. 15, 712 (1972) [JETP Lett. 15, 503 (1972)].
[12]D. F. Dance, M. F. A. Harrison, and A. C. H. Smith, Proc. R. Soc. Lond. A 290, 74 (1966).
[13]B. Peart and K. T. Dolder, J. Phys. B 6, 2415 (1973).
[14]E. Hinnov, T. K. Chu, H. Hendel, and L. C. Johnson, Phys. Rev. 185, 207 (1969).
[15]A. Burgess and V. B. Sheorey, J. Phys. B (to be published).
[16]D. Petrini, C. R. Acad. Sci. (Paris) 260, 4929 (1965).
[17]P. O. Taylor, Ph.D. thesis (University of Colorado, 1972) (unpublished) (available through University Microfilms Inc.).
[18]P. O. Taylor, K. T. Dolder, W. E. Kauppila, and G. H. Dunn, Rev. Sci. Instrum. 45, 538 (1974).
[19]M. D. Scherr, National Bureau of Standards, Washington (private communication).
[20]W. A. Shurcliff and S. S. Ballard, *Polarized Light* (Van Nostrand, New York, 1964), p. 69.
[21]B. M. Miles and W. L. Wiese, At. Data 1, 1 (1969).
[22]Report of Calibration, NBS Test No. 221.12-1B/72 (1972) (unpublished).
[23]We have had experience with several calibration standards, including the strip lamp calibrated by NBS, several Cu point black bodies built after the design of Lee [U. S. Natl. Bur. Stand., Technical Note 483 (1969)], a strip lamp calibrated by comparison against one of the black bodies, and recently a modified Cu point black body. Intercomparison of these standards at the 455.4- and 493.4-nm wavelengths gives agreement among all within 2%. Some difficulties with the low-temperature vacuum strip lamps (for example, 20% change in radiance with 1% change in current and guaranteeing identical geometry in use as in comparison to primary standards), make them less desirable than the black bodies as calibration standards. The strip lamp calibrated by NBS was considered the most reliable at the time calibration was performed, but a reliable modified Cu point black body developed since that time is about 1.6% brighter at the wavelengths of interest.
[24]I. C. Percival and M. J. Seaton, Philos. Trans. R. Soc. Lond. A 251, 113 (1958).
[25]D. R. Flower and M. J. Seaton, Proc. Phys. Soc. Lond. 91, 59 (1967).
[26]U. Fano and J. H. Macek, Rev. Mod. Phys. 45, 553 (1973).
[27]W. R. S. Garton, W. H. Parkinson, and E. M. Reeves, Proc. Phys. Soc. Lond. 80, 860 (1962).
[28]W. R. S. Garton and K. Coding, Proc. Phys. Soc. Lond. 75, 87 (1959).
[29]R. D. Hudson, V. L. Carter, and P. A. Young, Phys. Rev. A 2, 643 (1970).
[30]V. J. Ehlers and A. Gallagher, Phys. Rev. A 7, 1573 (1973).
[31]D. L. Moores and D. W. Norcross, J. Phys. B 5, 1482 (1972).
[32]E. A. Enemark and A. Gallagher, Phys. Rev. A 6, 192 (1972).
[33]See, for example, S. Geltman, *Topics in Atomic Collision Theory* (Academic, New York, 1969), Chap. 14.
[34]B. L. Moiseiwitsch and S. J. Smith, Rev. Mod. Phys. 40, 238 (1968).
[35]I. P. Zapesochnyĭ and L. L. Shimon, Dokl. Akad. Nauk. SSSR 166, 320 (1968) [Sov. Phys.—Dokl. 11, 44 (1966)].
[36]G. J. Schulz, Rev. Mod. Phys. 45, 378 (1973).
[37]A. Gallagher, Phys. Rev. 157, 24 (1967).
[38]E. Hinnov, 1973 (private communication).